Inertial scaling of dissipation in unsteady breaking waves

D A V I D   A.   D R A Z E N †,
W.   K E N D A L L   M E L V I L L E   AND   L U C   L E N A I N

Scripps Institution of Oceanography, University of California, San Diego, La Jolla,
CA 92093-0213, USA

Wave dissipation by breaking, or the energy transfer from the surface wave field to currents and turbulence, is one of the least understood components of air–sea interaction. It is important for a better understanding of the coupling between the surface wave field and the upper layers of the ocean and for improved surface-wave prediction schemes. Simple scaling arguments show that the wave dissipation per unit length of breaking crest, ϵ_l, should be proportional to $\rho_w g c^5$, where ρ_w is the density of water, g is the acceleration due to gravity and c is the phase speed of the breaking wave. The proportionality factor, or 'breaking parameter' b, has been poorly constrained by experiments and field measurements, although our earlier work has suggested that it should be dependent on measures of the wave slope and spectral bandwidth. In this paper we describe inertial scaling arguments for the energy lost by plunging breakers which predict that the breaking parameter $b = \beta(hk)^{5/2}$, where hk is a local breaking slope parameter, and β is a parameter of $O(1)$. This prediction is tested with laboratory measurements of breaking due to dispersive focusing of wave packets in a wave channel. Good agreement is found within the scatter of the data. We also find that if an integral linear measure of the maximum slope of the wave packet, S, is used instead of hk, then $b \propto S^{2.77}$ gives better agreement with the data. During the final preparation of this paper we became aware of similar experiments by Banner & Peirson (2007) concentrating on the threshold for breaking at lower wave slopes, using a measure of the rate of focusing of wave energy to correlate measurements of b. We discuss the significance of these results in the context of recent measurements and modelling of surface wave processes.

1. Introduction

Breaking waves play a significant role in the kinematics and dynamics of the surface wave field and the air–sea boundary layers, and therefore in many aspects of air–sea interaction. Breaking transfers momentum and energy from waves to currents, and energy to near-surface turbulence that is available for mixing the surface layers of the ocean. Heat and mass (e.g. gas, aerosol) transfer is enhanced by breaking. These and other aspects of breaking have been covered in periodic reviews of the subject (Banner & Peregrine 1993; Melville 1996; Duncan 2001). Notwithstanding the progress in measuring breaking in both the field and the laboratory, it still presents

† Present address: Naval Surface Warfare Center, Carderock Division, 9500 MacArthur Blvd, West Bethesda, MD 20817, USA.

formidable challenges to the experimentalist, the theoretician and the numerical modeller. Thus even simple scaling arguments, which can bring some order to the measurements, can be particularly valuable. In this paper, we present measurements of, and an inertial scaling argument for, the wave dissipation due to breaking which depend on a measure of the wave slope at breaking. The measurements and scaling also relate the kinematics of breaking to the dynamics.

With the advent of high-resolution coupled atmosphere–ocean numerical models, the role of surface-wave processes in air–sea interaction has drawn more attention in recent years. Wind–wave models are usually posed through the use of a radiative transfer equation (Komen, Hasselmann & Hasselmann 1984; Phillips 1985):

$$\frac{\partial N}{\partial t} + (c_g + U) \cdot \nabla N = S_{nl} + S_{in} + S_{diss}, \tag{1.1}$$

where $N(k) = g\psi(k)/\sigma$ is the action spectral density, $\psi(k)$ is the energy spectral density, k is the wavenumber, and σ is the intrinsic frequency. S_{nl}, S_{in} and S_{diss} are the 'source' terms for nonlinear interactions, wind input and dissipation, respectively. Of these terms, the dissipation is perhaps the least understood and is assumed to be dominated by wave-breaking processes. Models for S_{diss} are largely heuristic and 'tuned' to give agreement with the available data sets.

Phillips (1985) was the first to attempt to use a statistical description of the kinematics and dynamics of breaking to infer breaking statistics from the dynamical predictions of an equilibrium wave model. He introduced $\Lambda(c)$ so that $\Lambda(c) \, dc$ is the average total length of breaking fronts per unit surface area travelling with velocities in the range $(c, c + dc)$. Following Duncan (1981; see also Lighthill (1978, p. 459) on the wavemaking power of a cylinder), the average rate of energy loss for breaking waves with speeds in the range $(c, c + dc)$ was then given as

$$\epsilon(c) \, dc = b\rho_w g^{-1} c^5 \Lambda(c) \, dc, \tag{1.2}$$

where ρ_w is the density of water, g is acceleration due to gravity and the 'breaking parameter', b, was assumed to be constant by Phillips (1985) using a value of $b = 0.06$.

Duncan (1981) had studied quasi-steady breaking waves in the laboratory generated by a submerged hydrofoil. Through analysis of the horizontal and vertical momentum balances he arrived at the following scaling for the dissipation rate,

$$\epsilon_l = 0.009 \frac{\rho_w c^5}{g \sin \theta}. \tag{1.3}$$

Here ϵ_l is the dissipation per unit length of crest, c the phase speed of the wave, and θ the angle of inclination of the breaking region to the horizontal (see figure 1a). For the range of θ in the experiments, $\epsilon = b\rho_w c^5/g$ with the breaking parameter, $b = 0.044 \pm 0.008$. Subsequent work by Duncan (1983) to further resolve the drag on the hydrofoil showed a marked change in θ with varying hydrofoil depth. The results from this later work implied a broader range for b: 0.032–0.075. A summary of various estimates of the breaking parameter found in the literature is given in figure 2.

Measurements of the loss of momentum and energy fluxes from surface waves owing to unsteady breaking were performed by Rapp & Melville (1990, hereinafter RM). Implicit in RM's identification of a characteristic slope threshold for dissipation due to breaking is the fact that b must tend to zero for sufficiently small slopes. However, measured values of b approaching zero will be subject to the uncertainty associated with measurement errors and the expected transition from the generation of highly
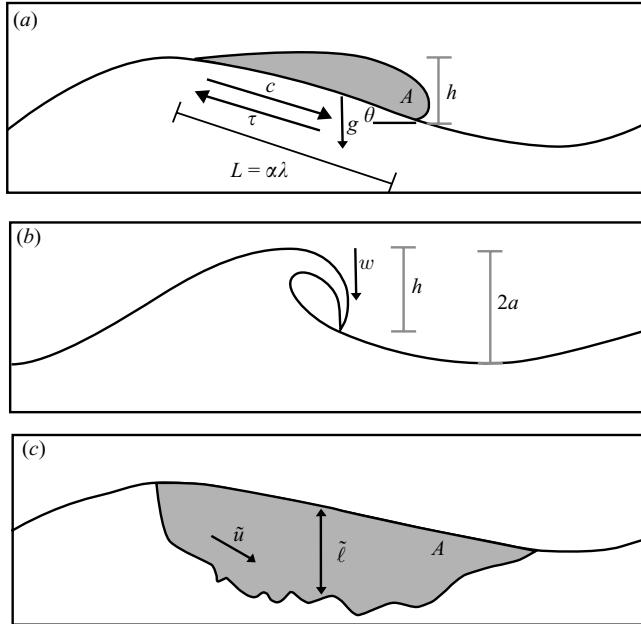
FIGURE 1. A definition sketch for (*a*) a spilling wave, (*b*) a plunging wave before breaking, and (*c*) a plunging wave after breaking. In (*a*) L is the length of the breaking region, λ the wavelength of the breaking wave, c the phase speed of the breaking wave, τ the shear stress exerted by the breaking region on the underlying fluid, g acceleration due to gravity, θ the angle of inclination, and A the area encompassed by the spilling wave. In (*b*) h is the height of the breaking region, $2a$ is the distance from the crest to the trough, and w is the representative velocity scale (the vertical speed of the falling wave tip). In (*c*) $\tilde{u}$ and $\tilde{\ell}$ are representative scales of the turbulence, and A the area encompassed by the post-breaking turbulent cloud.

dissipative parasitic capillary waves (Fedorov & Melville 1998) and breaking. RM found that up to 30 % of the initial energy of a wave packet could be lost through breaking of an individual wave and showed that approximately 90 % of the energy loss occurred within the first four wave periods after breaking. Analysis of the growth of the turbulent patch generated by breaking showed that the depth of mixing was of the order of the breaking wave height. Lamarre & Melville (1991) showed that up to 50 % of the energy lost was due to work done in entraining air against buoyancy forces. The large levels of energy lost along with high void fractions suggest that the post-breaking region is well-mixed and highly dissipative.

Melville (1994) undertook a re-analysis of the data of Loewen (1991) to find that the non-dimensional dissipation rate b, which varied approximately linearly with an integral measure of the slope of the wave packet, was in the range, $b = [4-12] \times 10^{-3}$. The slope was defined as the maximum slope at focusing according to linear theory, or the sum of all the component slopes, $S = \sum_{n=1}^{N} a_n k_n$, where a_n and k_n are the amplitude and wavenumber, respectively, of the Fourier components. Using an inertial estimate of the viscous dissipation rate in turbulence, $\epsilon \approx u^3/l$, with u and l representative velocity and length scales, respectively, of the turbulent cloud generated by breaking, Melville obtained $b = [3-16] \times 10^{-3}$ based on scaling arguments from RM. The correlation between these two measures of b is quite good considering that the argument used is based on an order-of-magnitude estimate.
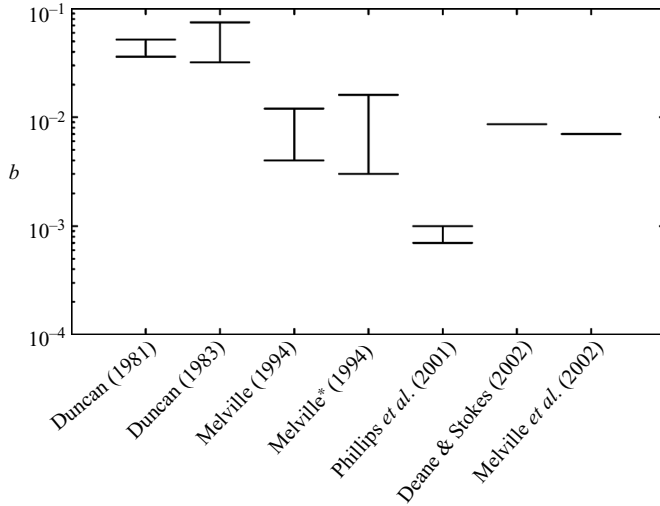
FIGURE 2. Estimates of b from the literature. See table below for details. All quasi-steady and unsteady assumptions refer to laboratory measurements of b.

Experiments	b	Measurement details
Duncan (1981)	$[4.4 \pm 0.8] \times 10^{-2}$	Quasi-steady breaking
Duncan (1983)	$[3.2, 7.5] \times 10^{-2}$	Quasi-steady breaking
Melville (1994)	$[4, 12] \times 10^{-3}$	Unsteady breaking
Melville*(1994)	$[3, 16] \times 10^{-3}$	Inferred from $\epsilon \approx u^3/l$
Phillips et al. (2001)	$[7, 10] \times 10^{-4}$	Remote field measurements
Deane & Stokes (2002)	8.6×10^{-3}	Unsteady breaking
Melville et al. (2002)	7×10^{-3}	Unsteady breaking

Through analysis of radar measurements of wind-generated ocean waves, Phillips, Posner & Hansen (2001) inferred an estimate of $b = [7 - 13] \times 10^{-4}$. The indirect method of measurement made it difficult at times to distinguish individual breaking events, especially when they were being overtaken by faster events. This could account for the lower levels of b seen relative to those in the laboratory. The upper limits of these estimates of b, however, are close to the lower range of Melville (1994) and would be consistent with weaker breaking events (see the discussion in §6).

Deane & Stokes (2002) measured bubble size distributions within a breaking wave in seawater in the laboratory. Assuming the turbulent velocity field to be within an inertial subrange, the authors found that $a_H \propto \epsilon^{-2/5}$, where a_H is the Hinze scale, the smallest size of bubble undergoing fragmentation by the turbulence, and ϵ is the viscous dissipation. Based on their results, they computed $\epsilon_l = 12.46 \, \mathrm{kg \, m \, s^{-3}}$, yielding $b = 8.6 \times 10^{-3}$. They state that the breaking event considered was a multiple breaking event, which is consistent with the range of b found for multiple breaking events in Melville (1994).

Melville, Veron & White (2002) undertook measurements of the evolution of the turbulence generated by unsteady breaking waves in the laboratory using dispersive focusing of a wave packet, and particle image velocimetry (PIV) to measure the turbulent velocity field. For those experiments at one particular value of S it was found that $b = 7 \times 10^{-3}$.

These measurements of b in the literature are summarized and tabulated in figure 2. It can be seen that the values fall into three classes, which are in descending magnitude of b: quasi-steady spilling waves; unsteady breaking due to dispersive focusing; and remote field observations combined with wave modelling.

The importance of b is that it provides a quantitative relationship between the kinematics of breaking, represented by the speed of the breaker, c, and the dynamics, represented by the loss of wave energy (dissipation) or the momentum flux from waves to currents. Using airborne imagery of whitecaps, Melville & Matusov (2002) measured $\Lambda(c)$, and its lower moments were calculated. As shown above, the dissipation is proportional to the fifth moment with $b\rho_w/g$ as the proportionality factor. In Melville & Matusov (2002), the distribution of momentum flux and energy dissipation as a function of c were inferred using a constant $b = 8.5 \times 10^{-3}$ and error bars encompassing the measurements of Melville (1994). However, it is clear from that work that the shape of these distributions would be significantly affected if there were a correlation between b and c, perhaps through the wave slope.

Modelling of breaking is also dependent on a better understanding of b and its dependence on wave-field variables. Sullivan, McWilliams & Melville (2004) developed a stochastic model of breaking waves on the ocean surface and evaluated the model through the use of direct numerical simulation, DNS. The model was based on the Navier–Stokes equations with an additional forcing term, A, that represents the accelerations induced by breaking. The breaking was randomly added to the surface of the domain with a specified whitecap coverage. The forcing A was modelled on the laboratory results of RM and Melville *et al.* (2002), as well as the field measurements of Melville & Matusov (2002). Sullivan *et al.* (2004) found that the model agreed well with experimental data from a single unsteady breaking wave (Melville *et al.* 2002). Additionally, they found that with just a small fraction of active breaking there was significant turbulent mixing and transport of vertical momentum. Sullivan, McWilliams & Melville (2007) have further developed the numerical model with large-eddy simulations (LES) including both stochastic breaking and vortex force terms. They find that the synergy between wave breaking and Langmuir circulations, or Langmuir turbulence, can lead to the effects of breaking being felt to depths comparable to the vertical scale of the Langmuir circulations.

Melville (1994) showed with simple dimensional analysis of laboratory experiments on unsteady breaking due to dispersive focusing that at sufficiently large Reynolds numbers, the breaking parameter b should be a function of both a characteristic slope and bandwidth of the wave packet prior to breaking. Over a limited range of wave slopes, it was found that for single breaking events b increased with the slope parameter, but no attempt was made to derive a functional relationship for the slope dependence.

In §2, we review the dimensional analysis of the dissipation rate and propose a slope-dependent model of ϵ_l for plunging breaking waves. In §3, the experimental set-up is described. The measurement of the dissipation rate is described in §4, §5 presents the experimental results, while §6 discusses these results and the results of Banner & Peirson (2007) and their implications for field measurements.

2. Scaling of the dissipation rate

2.1. *Dimensional analysis for the wave packet*

Consider a two-dimensional wave packet, which according to linear wave theory would focus or 'break' at (x_b, t_b). Here x is the downstream distance and t is time,

both from arbitrary origins. We can express the dependent variables, including for example the velocity field, as

$$\boldsymbol{u} = \boldsymbol{u}(\boldsymbol{x}, t; \rho_w, \rho_a, g, \Gamma, a, k, \Delta k, \mu_w, \mu_a), \tag{2.1}$$

where ρ_w is the density of water, ρ_a the density of air, g gravity, Γ surface tension, a the characteristic wave amplitude, k the characteristic wavenumber, and μ_w, μ_a the viscosity of water and air, respectively. Of particular interest is the dissipation of wave energy per unit length of breaking crest, ϵ_l (not to be confused with the viscous dissipation of mechanical energy into heat), which can be expressed as a function of time with a parametric dependence on the other variables described immediately above. Dimensional analysis then gives

$$\frac{\epsilon_l}{\rho_w c^5/g} = fn\left(\frac{t}{T}; Bo, Re_a, Re_w, ak, \frac{\Delta k}{k}, \frac{\rho_a}{\rho_w}\right), \tag{2.2}$$

where $c = (g/k)^{1/2}$ is the characteristic phase speed and $T = 2\pi/(gk)^{1/2}$ is the characteristic period of linear deep-water gravity waves, $Re_w = 2\pi c\rho_w/k\mu_w$, $Re_a = 2\pi c\rho_a/k\mu_a$ are the Reynolds numbers for the water and air, respectively, and $Bo = \rho g/\Gamma k^2$ is the Bond number.

We assume that the flow becomes independent of the Reynolds numbers for sufficiently large values of Re. For the flows considered here, Reynolds numbers for water and air are $O(10^5 - 10^6)$ and $O(10^4 - 10^5)$, respectively. If we also restrict consideration to air–water systems close to standard temperature and pressure, the air–water density ratio and Bond number remain effectively constant and (2.2) depends on a characteristic wave packet slope, ak, and bandwidth, $\Delta k/k$. Thus we have,

$$\frac{\epsilon_l}{\rho_w c^5/g} = f_n\left(\frac{t}{T}; ak, \frac{\Delta k}{k}\right). \tag{2.3}$$

This dimensional analysis, which is consistent with the earlier analysis of RM, demonstrates that the dominant dimensionless variables describing the dissipation of wave energy by breaking are the wave-packet slope and the bandwidth. The general significance of the wave slope in describing breaking has been known from laboratory, field and numerical studies for a long time, so long in fact that it is difficult to trace its origins. However, detailed knowledge of the dependence of the dissipation on slope has been lacking. The definition of the slope parameter has varied as well from local slopes used as 'breaking criteria' to integral measures of the slope based on the peak frequencies (or wavenumbers) of wave spectra and significant wave heights: the 'significant slope'. Here, we have defined the characteristic slope to be the maximum slope that a linearly focusing wave packet would attain. The reciprocal of the bandwidth is a dimensionless measure of the width of the wave packet. The larger the bandwidth, the narrower the wave packet at focusing.

2.2. *Local dimensional analysis and scaling of dissipation for plunging waves*

Figure 3 shows images taken from a high-speed video of plunging breaking waves in the laboratory, with figure 3(*a*) corresponding to the time the surface becomes vertical and the toe at the crest begins to form. Figure 3(*b*) corresponds to incipient impact of the toe of the breaker on the surface below. Between figures 3(*a*) and 3(*b*) the toe has travelled a vertical distance, h. The time between each image is $\Delta t = (h/2g)^{1/2}$.
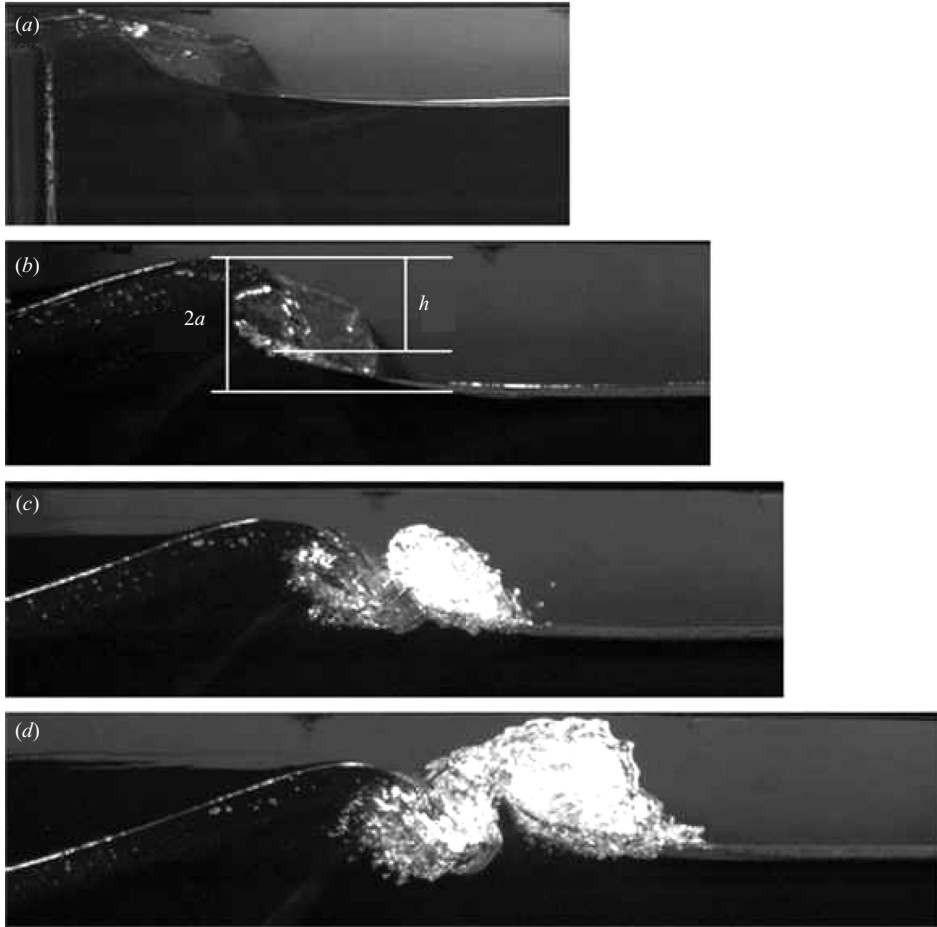
FIGURE 3. A sequence of stills from a high-speed video of a plunging breaking wave. The time between adjacent images is $\Delta t = (h/2g)^{1/2}$. (b) is the time at which impact occurs.

Melville (1994) showed that use of the inertial estimate of turbulent dissipation in the post-breaking turbulent cloud, $\epsilon \approx u^3/l$, yields estimates of the breaking parameter b which agree with those based on the laboratory measurements of Loewen (1991), but it provided no explicit dependence on the wave slope.

An inertial model of the dissipation rate is sought for plunging waves with the local wave height h and velocity at impact as the length and velocity scales of the flow. Using a plunging breaking wave as our model, we assume that the toe of the breaking wave falls through a height h (figure 1b). Figure 4 shows the trajectory of the toe of a plunging breaking wave as measured by a high speed camera. The elevation is the height above the impact point and the time origin is when the toe of the breaking wave first appears. The solid line is the elevation of the toe of the breaker on a ballistic trajectory under gravity, $z = z_0 - g(t - t_0)^2/2$, where t_0 is the time of maximum elevation, z_0. These results show that to a good approximation the toe is in freefall under gravity. The vertical velocity of the toe at impact on the surface below is then
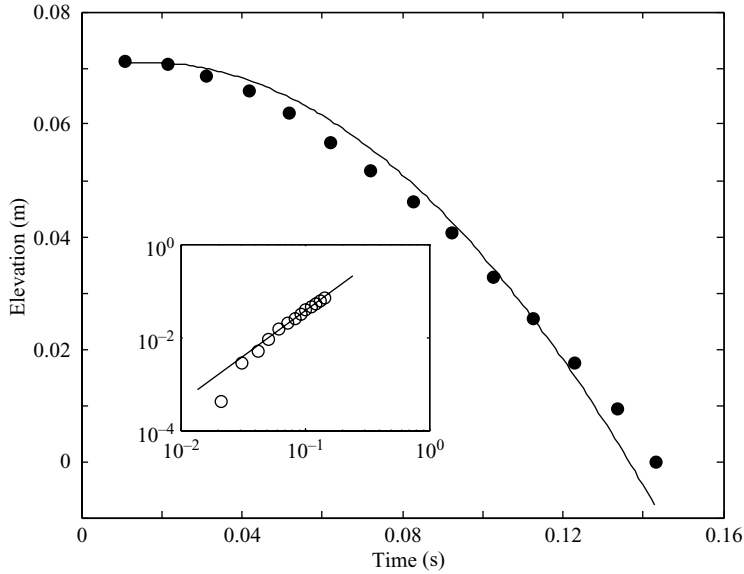
$$w = (2gh)^{1/2}, \tag{2.4}$$

FIGURE 4. Location of the toe of a plunging breaking wave with the ballistic trajectory (solid line) as predicted by projectile motion, $g/2\,(t - t_0)^2$ where t_0 is the point of maximum elevation. Time equal to zero is the time of initial toe formation. Elevation is the height above the point where the toe impacts the water surface. The distance between the first and last points shown here is h (defined in figure 1). The inset figure is the distance the tip has fallen with logarithmic axes, the solid line shown has a slope of 2.

and h is the length scale of the volume of fluid that will collapse under gravity into a turbulent cloud. The time for the toe to travel from the crest to the impact point is just $\tau = (h/2g)^{1/2}$.

Now RM showed that up to 90 % of the viscous dissipation of wave energy occurs in the first few wave periods. If we assume that most of this viscous dissipation occurs during the time that the wave is actively breaking, then we would be able to use the inertial estimate of viscous dissipation to scale the wave dissipation too. For this cloud of turbulence, the dissipation per unit mass should scale with

$$\epsilon = \chi \left(\frac{w^3}{h} \right) = \chi (2g)^{3/2} h^{1/2}, \tag{2.5}$$

where χ is a constant of $O(1)$. The dissipation per unit length along the wave crest is simply

$$\epsilon_l = \rho_w A \epsilon = \chi \rho_w \frac{\pi}{4} h^2 (2g)^{3/2} h^{1/2} \tag{2.6}$$

$$= \chi \frac{\pi}{\sqrt{2}} \rho_w g^{3/2} h^{5/2}, \tag{2.7}$$

where for definiteness we have assumed a cylindrical cloud of turbulence of cross-sectional area $A = \pi h^2 / 4$. See figure 3(d) and Melville (1996, figure 2).

Expressing (2.7) as

$$\epsilon_l = \frac{b \rho_w c^5}{g}, \tag{2.8}$$

and using the linear dispersion relationship gives

$$b = \chi \frac{\pi}{\sqrt{2}}(hk)^{5/2} = \beta(hk)^{5/2}, \tag{2.9}$$

where χ and β are constants of order unity. Thus we can see that this model predicts that b should have a dependence on a slope parameter, hk which we call the local slope at breaking.

With the benefit of the previous argument, we can now consider an even simpler hypothesis regarding the dependence of the wave dissipation rate, ϵ_l, on the local geometry of the plunging breaker. We assume that

$$\epsilon_l = \epsilon_l(\rho_w, g, h). \tag{2.10}$$

Implicit in this formulation is an assumption of geometrical similarity of the toe of the breaker scaled by h, that the toe follows a ballistic trajectory represented by g, and that the initial velocity of the toe relative to the underlying wave is a small fraction of the phase speed of the wave, see also Van Dorn & Pazan (1975) and Perlin, He & Bernal (1996). With four variables and three dimensions it follows that the relationship contains only one dimensionless group, in consequence of which

$$\frac{\epsilon_l}{\rho_w g^{3/2} h^{5/2}} = C, \tag{2.11}$$

where C is a constant.

Introducing the wavenumber k, and the linear dispersion relationship, this is equivalent to

$$\epsilon_l = C \frac{\rho_w c^5 (hk)^{5/2}}{g}; \tag{2.12}$$

the same result as the inertial argument above. Without the inertial argument for physical support, or the empirical evidence to be presented below, it is unlikely that such a dimensional analysis would have much credence, nor would the magnitude of the constant, C, be constrained, but it serves to demonstrate the minimal set of parameters that give the inertial result.

The experiments described below were conducted to test (2.9). Additional experiments were performed to measure directly the post-breaking turbulence and vorticity fields and are reported in Drazen (2006) and Drazen & Melville (2008).

3. Experimental set-up

3.1. *Facilities*

The experiments were performed using the small glass channel in the Hydraulics Laboratory at the Scripps Institution of Oceanography (SIO). The tank is 30 m long, 0.5 m wide, and 1 m deep. Waves are generated by a computer-controlled hydraulically driven wavemaker at one end of the tank and are dissipated on a beach of 6° slope covered with a thick fibrous mat (figure 5). The toe of the beach starts 24.5 m from the resting position of the wavemaker and the tank was filled to a working depth of 0.6 m with fresh water.

3.2. *Packet generation*

The wavemaker was programmed to generate a breaking event at (x_b, t_b) using dispersive focusing, a technique initially proposed by Longuet-Higgins (1974). Each
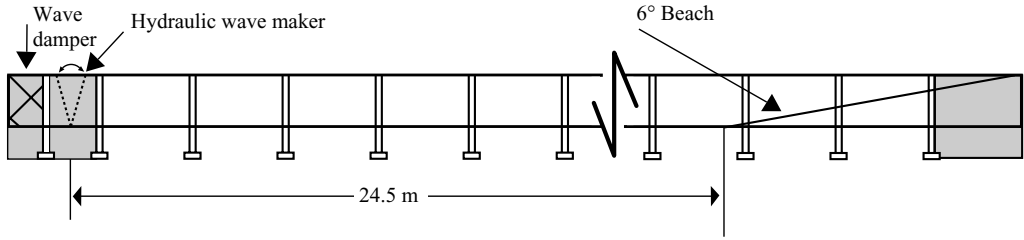
FIGURE 5. Schematic diagram showing the small glass channel in the Hydraulics Laboratory at the Scripps Institution of Oceanography.

wave packet has 32 separate frequency components spread across a bandwidth of $\Delta f/f_c$ centred at the frequency f_c. Further details on the generation of a breaking wave packet can be found in RM. The formulation here varies from that of RM in that the slope of each component is a constant as in Loewen & Melville (1991). The maximum slope given by linear theory is $S = \sum_{n=1}^{N} a_n k_n$ and will be referred to as the input slope. It has been shown *a priori* by RM that the significant non-dimensional parameters for describing wave dissipation are S, $\Delta f/f_c$, and $x_b k_c$, and our parameter space will be defined by these quantities. Empirically, RM found no significant dependence on $x_b k_c$; a result confirmed below. For the experiments described here, we varied the centre frequency over $f_c = [0.88, 1.08, 1.28]$ Hz, the bandwidth over $\Delta f/f_c = [0.5, 0.75, 1.00]$, and the breaking location over $x_b k_c = [28.5, 41.50, 57.92]$. For each of these 27 total cases the range of the input slope varied over $S = [0.28 : 0.02 : 0.54]$.

3.3. *Measurements*

Surface wave heights in the channel were measured with an array of seven resistance wire wave gauges using impedance-measuring electronics from the Danish Hydraulics Institute (Model 80-74G). Each gauge consisted of a pair of 0.25 mm diameter Nichrome 80 wires spaced 5 mm apart mounted to the channel from above with a rack and pinion which allowed precise vertical positioning of the instrument. During the course of the experiments the gauges were placed along the midline of the tank and spaced approximately 3 m apart to minimize any flow disturbance on downstream gauges. For a given set of experimental conditions, the six downstream wave gauges were shifted by 1 m while the first gauge remained fixed to serve as a control. This was repeated until the desired spatial resolution was obtained along the channel.

The seven wave gauges, one hydrophone, the input signal to the wavemaker and the wavemaker position were each sampled at 10 kHz with an inter-channel delay of 1 μs. Thus the maximum delay between channels was at most 10 μs, which is negligible for this kind of data. The high sampling rate was dictated by the hydrophone, which measured the acoustical signature of the breaking wave in order to obtain a measure of the duration of breaking. The hydrophone (International Transducer Corp., ITC-6050C) was located 20 cm off the floor of the tank at a distance of 4.96 m from the wave paddle. Prior to analysis, the surface elevation time series were resampled at 100 Hz. Between repeats of the experiment, the control system wrote the data to hard disk and waited 8 min for the wave channel to settle. For further details see Drazen (2006, Appendix A). The repeatability of the amplitude and phase of the surface elevation is within 1 mm, and 1 ms or 0.1 % of the wave period.

Results from Loewen (1991) (see also Deane & Stokes 2002) showed that there was still significant energy in the hydrophone signal for frequencies above 5 kHz.
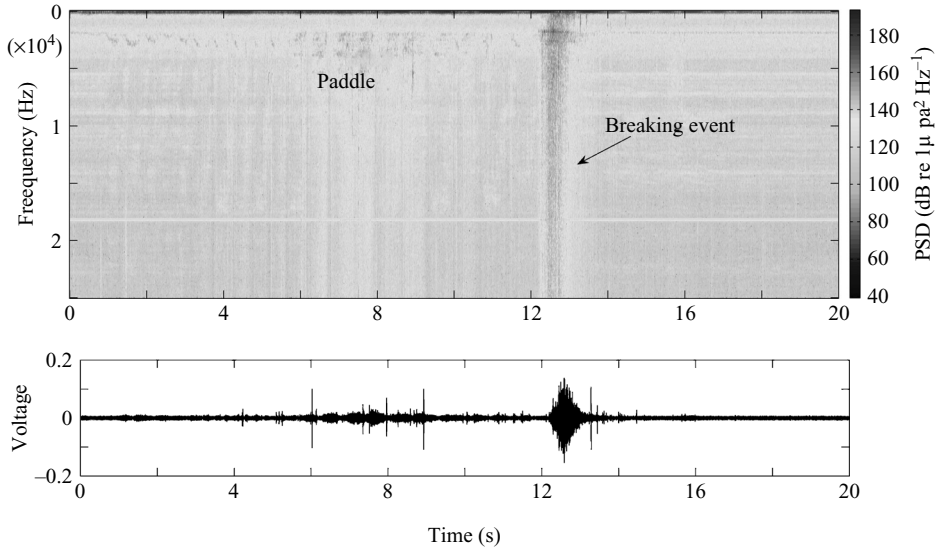
FIGURE 6. (*a*) Spectrogram and (*b*) voltage time-history of a hydrophone signal. The breaking event is seen as a broadbanded signal in the spectrogram.

For a series of experiments devoted to the use of the hydrophone to more accurately measure the duration of active breaking, it was recorded at 50 kHz along with one wave gauge as a control for checking repeatability. The duration of the breaking event is determined by differencing the start and stop times of breaking from the spectrogram of the hydrophone signal (figure 6). This yields an estimate of the duration of active breaking, τ_b, during which the wave impacts the water surface, air is entrained, and bubbles fragment (Lamarre & Melville 1991; Loewen & Melville 1991; Deane & Stokes 2002).

A megapixel video camera (Pulnix TM-1040), was used to record video imagery of the wave at the breaking location. The camera was run at a maximum frame rate of 30 Hz and the images were then saved as bitmaps to the hard drive. Analysis of the images permitted measurement of the wave height, $2a$, the location of the breaking event relative to the wave paddle, x_b, and the local height of the breaking surface h. The height over which the wave breaks, h, for a plunging wave is well defined, but less so for a spilling wave. For spilling breakers we define h to be the vertical extent of the spilling region as in figure 1(*a*). This varies in time and is more prone to measurement error than is h for plunging waves, but is taken to be the maximum vertical extent of the spilling region. From these spatial measurements at breaking we define two slopes, the local slope, hk_c where k_c is the centre wavenumber of the packet, and a slope based on the local amplitude, ak_c. To remove any potential bias error, measurement of h was performed six times on the video imagery, the highest and lowest values were removed, and a mean was taken over the remaining four measurements for each wave case.

4. Measurement of the dissipation rate

In order to measure the energy loss from breaking, the approach developed by RM is used. A packet of waves propagating down the tank is shown in figure 7. As the wave packet approaches the theoretical breaking location, it can be seen to
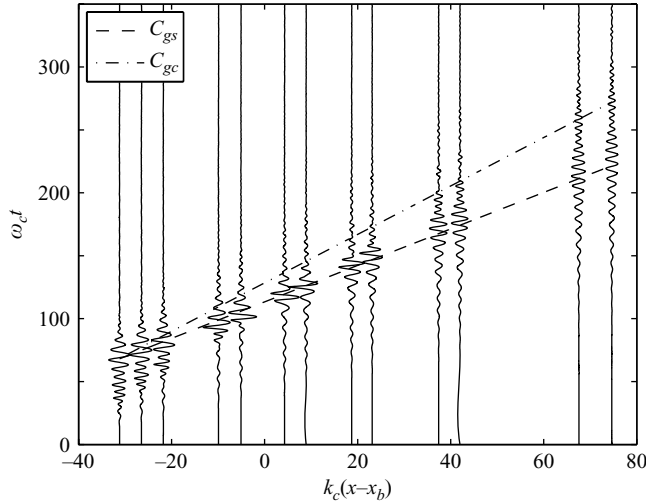
FIGURE 7. A plot showing time series of surface elevation at a number of locations in the tank. Superimposed on top of the surface elevation are the group velocity lines corresponding to the centre wave component C_{gc} and the spectrally weighted group velocity C_{gs} as defined in the text, (4.5). The packet parameters are $f_c = 1.08$ Hz, $\Delta f/f_c = 0.75$, $x_b k_c = 41.50$, $S = 0.34$. Note that the vertical scale of the time series are exaggerated relative to the horizontal scale on the graph.

steepen, break, and then disperse as it moves downstream. At each gauge location, the time-integrated potential energy per unit length can be calculated

$$E_p = \frac{1}{2} \int_{t_1}^{t_2} \rho_w g \eta^2 \, \mathrm{d}t, \tag{4.1}$$

where η is the surface elevation, and the range $[t_1, t_2]$ encompasses the wave packet.

We now consider a control volume with boundaries far upstream and downstream of breaking at which we assume equipartition of energy. (Equipartition is not likely to be a good approximation at or near breaking.) Thus at these locations the energy density is equal to twice the potential energy density,

$$E = \rho_w g \overline{\eta^2}, \tag{4.2}$$

where the overbar represents an average over the local wavelength. The change in energy flux through this control volume over the time $t = t_1 \rightarrow t_2$ can be written as

$$\Delta F = \int_{t_1}^{t_2} C_{g_2} \rho_w g \eta_2^2 \mathrm{d}t - \int_{t_1}^{t_2} C_{g_1} \rho_w g \eta_1^2 \, \mathrm{d}t, \tag{4.3}$$

where (C_{g_1}, η_1) and (C_{g_2}, η_2) are characteristic group velocities and the surface elevations at the upstream and downstream boundaries of the control volume.

We must now define the characteristic group velocity of the wave packet in order to apply (4.3). The group velocity of a component of the wave packet is given by

$$C_g = \left. \frac{\partial \sigma}{\partial k} \right|_c = \frac{1}{2\sigma} \left[\frac{\sigma^2 + gk^2 h(1 - \tanh^2(kh))}{k} \right]. \tag{4.4}$$

The packet propagation more closely follows a weighted average of the group velocities (see figure 7) as defined by

$$C_{g_s} = \frac{\sum C_{g_n} a_n^2 \delta\sigma}{\sum a_n^2 \delta\sigma},$$ (4.5)

where C_{gs} is the spectrally weighted group velocity and a_n and C_{g_n} are the amplitude and group velocity of the nth component of the wave packet, and $\delta\sigma$ is the increment in frequency between components. Within the accuracy of the experiments we found that $C_{g_1} = C_{g_2} = C_{g_s}$ and (4.3) simplifies to

$$\Delta F = \rho_w g C_{g_s} \int_{t_1}^{t_2} \left(\eta_2^2 - \eta_1^2\right) \mathrm{d}t.$$ (4.6)

The normalized change in energy flux across the control volume is shown in figure 8. It can be seen that as the input slope is increased, the amount of energy lost increases quite rapidly once the wave begins breaking. The energy loss then begins to plateau at the onset of multiple breaking events. For the strongest case of single breaking, up to 35 % of the energy entering the volume is dissipated. Variations in the distance to breaking do not cause significant variation in the amount of energy lost which agrees with RM. However, we do see variations with changes in the packet bandwidth (figure 9) in contrast to the findings of RM, which are accompanied by changes in the qualitative nature of the breaking. While multiple breaking occurs for some cases in figure 9, analysis of the breaking parameter, b, will be undertaken for single breaking cases unless otherwise specified. As stated previously, the packets used in the experiments described are based upon a formulation in which each component has equal slope versus the constant-amplitude method of RM. We expect that this difference in initial data results in the detailed differences between RM and this work, including the dependence on the bandwidth.

We wish to evaluate the dissipation rate due to a single breaking event only. The loss due to breaking must be isolated from that due to non-breaking effects such as friction with the bottom and sidewalls of the tank. We will define the total change in energy flux within the control volume to be

$$\Delta F_{tot} = \Delta F_b + \Delta F_{nb},$$ (4.7)

where ΔF_b is the change due to breaking and ΔF_{nb} is the change due to non-breaking effects. The non-breaking effects are quantified by evaluating (4.6) for the incipient-breaking case.

The duration of the breaking increases as the input slope is increased and for all these data is of the order of one wave period. This is consistent with RM and Loewen & Melville (1991), who showed that the breaking duration is approximately one wave period, and that the time of active breaking correlates well with the duration of the hydrophone signal.

The average dissipation rate per unit length of crest can now be defined as

$$\epsilon_l = \frac{-\Delta F_b}{\tau_b} = \frac{\rho_w g C_{g_s} \int_{t_1}^{t_2} \left(\eta_1^2 - \eta_2^2\right) \mathrm{d}t}{\tau_b},$$ (4.8)

where τ_b is the duration of active breaking as measured by the hydrophone (figure 10).

5. Results

The measured dissipation rate is used in (2.8), with $c = c_c$, the phase speed at the centre frequency of the wave packet, to compute the breaking parameter b. This is
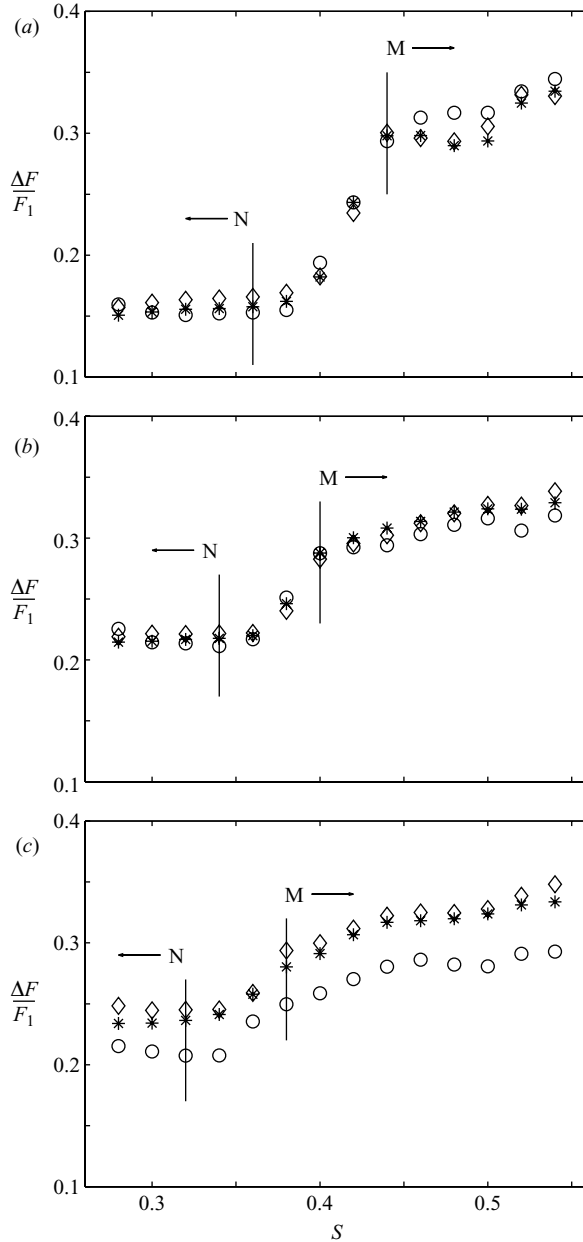
FIGURE 8. Normalized change in energy flux across the control volume as a function of input slope for (*a*) $f_c = 0.88$ Hz, (*b*) $f_c = 1.08$ Hz, (*c*) $f_c = 1.28$ Hz. Here, F_1 is the total energy entering the control volume at the furthest upstream location. All packets have $\Delta f/f_c = 0.75$ with $x_b k_c = 28.5\,(\circ)$, $x_b k_c = 41.50\,(\ast)$, and $x_b k_c = 57.92\,(\diamond)$. The regions where non-breaking events (N) and multiple breaking (M) occurs are also denoted.

shown as a function of input slope, S, in figure 11, along with the data of Loewen & Melville (1991) as reanalysed by Melville (1994). The solid line shows the mean of b over all parameter space for a given value of S.
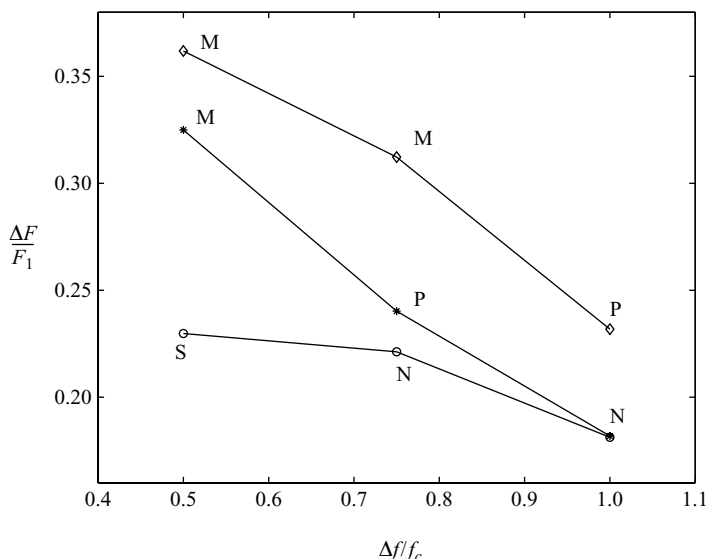
FIGURE 9. Normalized change in energy flux across the control volume as a function of bandwidth, with F_1 the total energy entering the control volume. All packets have $f_c = 1.08$ Hz and $x_b k_c = 57.92$ with $S = 0.32 (\circ)$, $S = 0.38 (*)$, and $S = 0.46 (\diamond)$. The qualitative nature of the breaking is also noted, where N is non-breaking, S is spilling, P is plunging, and M is multiple breaking.
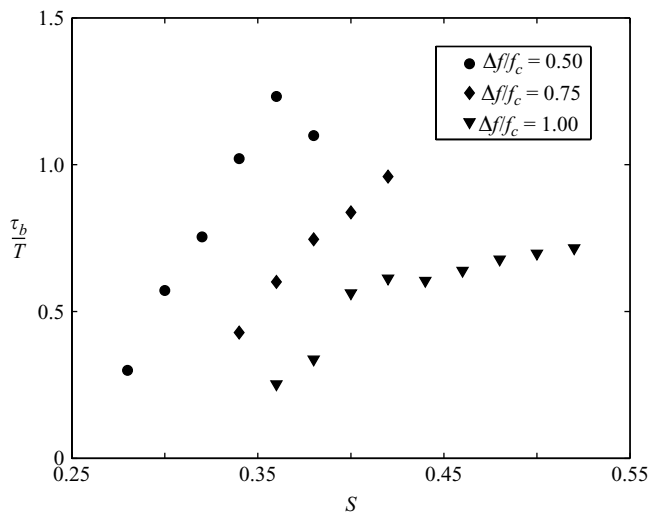

FIGURE 10. Normalized duration of single breaking (τ_b/T) versus input slope as measured from the hydrophone. Each data point is a mean taken for single breaking events over all f_c and $x_b k_c$ for a given value of $\Delta f/f_c$.

The error bars denote the standard deviation of the data at each S. The measurements of b from our data show a dependence on the input slope, which agrees with the findings of Melville (1994). However, for the range of slopes considered by Melville (1994), multiple breaking events begin at $S \approx 0.30$, where multiple breaking here does not start until $S \approx [0.36, 0.40, 0.52]$ for $\Delta f/f_c = [0.50, 0.75, 1.00]$. The two
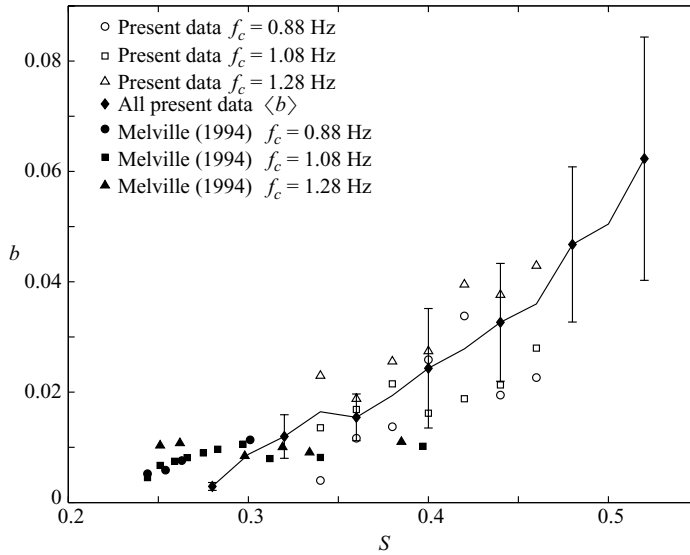
FIGURE 11. Plot of b versus S for similar experimental conditions as Melville (1994) for both single and multiple breaking waves. The diamonds represent $\langle b \rangle$, the mean of the data for all parameter space for a given slope, not just the subset considered here (see below). The error bars denote the standard deviation of b over all parameter space for a given value of S. The data of Melville (1994) are shown with filled black symbols and the present measurements are shown with open symbols. For both data sets we plot $f_c = 0.88$ Hz ($\circ$), $f_c = 1.08$ Hz ($\square$), $f_c = 1.28$ Hz ($\triangle$). For the present data, $\Delta f / f_c = 0.75$ and $x_b k_c = 28.5$ for all f_c, while for Melville (1994), $\Delta f / f_c = 0.73$ and $x_b k_c = 28.3$ for all f_c.

sets of experiments explored a similar range of parameter space, used wave tanks of nearly the same dimensions, and both used a constant-slope formulation in generating wave packets. The main difference between the two sets of experimental conditions is that the water depth for Loewen & Melville (1991) was 0.38 m as against 0.6 m used in the experiments described here. For the range of wavelengths considered in each experiment, kH was 1.35–2.54 for Loewen & Melville (1991) and 1.95–3.96 for the experiments described here, where H is the still-water depth. Thus a larger number of wave components experience shallow-water effects and will probably break at a lower value of S than for our data. Despite the quantitative differences between the measurements, the rate at which b increases for single breaking events is similar.

The effect of the other parameters on the dissipation rate is shown by looking at the variation in $\langle b \rangle$, the mean of b, taken over all parameter space for a given value of $\Delta f / f_c$ or $x_b k_c$, as shown in figure 12. The thin error bars represent the range between minimum and maximum values, while the thicker lines denote the standard deviation of the data. The dependence of b on the breaking location is seen to be negligible, but the bandwidth is significant and $\langle b \rangle$ increases with increasing $\Delta f / f_c$.

Figure 13 is a plot of the measured values of b for plunging waves only. The normalized dissipation rate, or breaking parameter, b, is consistent with an $hk_c^{5/2}$ dependence as predicted by (2.9). The values for spilling breakers are not shown here owing to the difficulty in assigning a single value of h to an unsteady spilling wave. In addition to the dependence on hk, agreement with (2.9) also requires that the factor β be $O(1)$. Fitting only the data for plunging waves to (2.9) we find that $\beta = [0.71, 0.99, 1.05]$ for $\Delta f / f = [0.5, 0.75, 1.0]$. Despite the scatter, the data support the inertial scaling argument both in dependence on hk_c and in the order of magnitude.
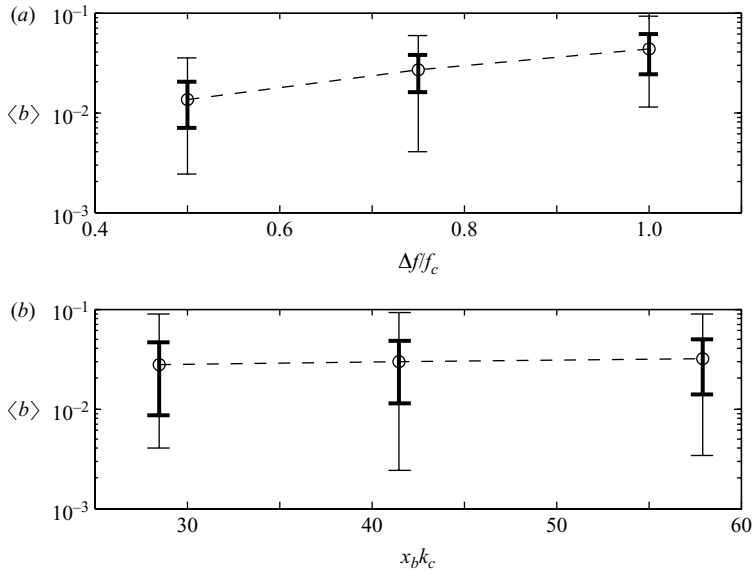
FIGURE 12. Plot of $\langle b \rangle$ versus (a) $\Delta f/f_c$ and (b) $x_b k_c$, where the average is over all samples for a given value of $\Delta f/f_c$ or $x_b k_c$. The thin error bars span the maximum and minimum values within the average, and the thicker line is the standard deviation of the data.
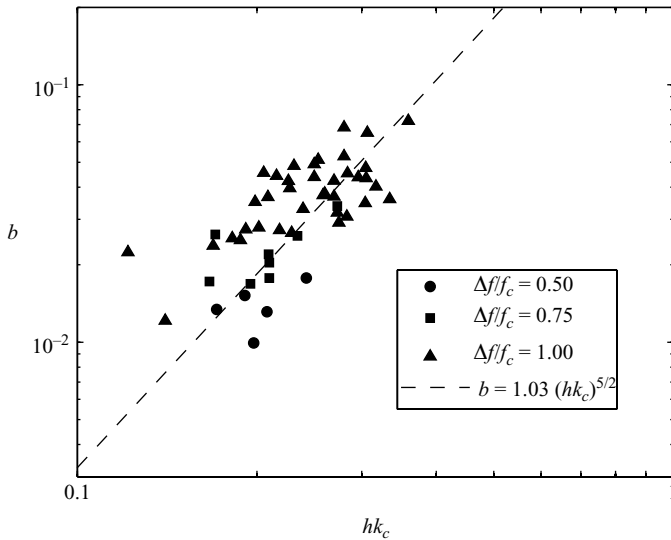

FIGURE 13. Plot of b versus the local slope, hk_c. Data for all three bandwidths for singly breaking plunging waves only are shown. The dashed line is a fit of the data to the curve $b = \alpha(hk_c)^{5/2}$, where $\alpha = 1.03$.

However, while the inertial argument for the dissipation rate and its support by the empirical data provides important insight into, and scaling of, the dissipation process, it provides no overall predictive capability since hk_c is not known *a priori*. What we do know *a priori* are the parameters describing the wave packet, so it is of interest to see whether they can be used to collapse the data.
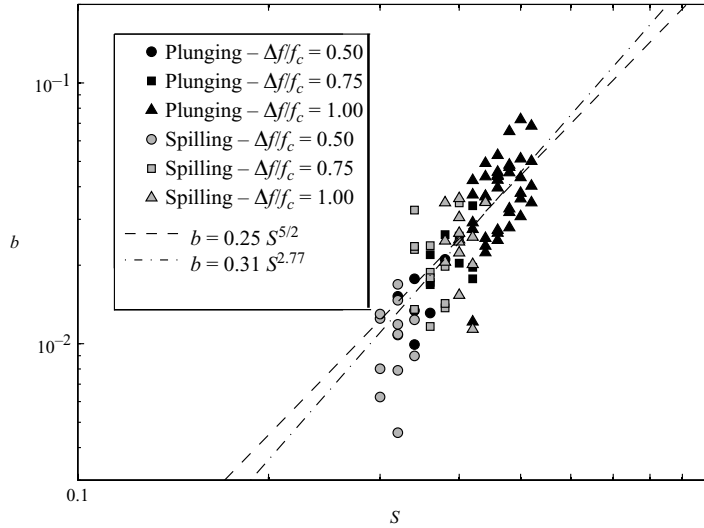
FIGURE 14. Plot of b versus the input slope, S for singly breaking plunging and spilling waves. The dashed line is a fit of the data to the curve $b = \alpha S^{5/2}$, where $\alpha = 0.25$. The dash-dot line is a fit to $b = \alpha S^n$ with $\alpha = 0.31$ and $n = 2.77$.

A plot of b versus the input wave packet slope, S, for both spilling and plunging waves is shown in figure 14. While linear theory is sufficiently accurate for experimental design; for example, predicting the break-point to within a wavelength, nonlinear effects become significant close to breaking. Thus we do not necessarily expect a linear relationship between the input slope S, which is the linear prediction of the maximum slope at focusing, and the local slope hk_c at breaking. Furthermore, h is the height of the plunging face of the wave at impact, or the vertical distance from the crest to the toe of the spilling breaker, not the full crest to trough height. Nevertheless, the least-squares fit of the data to $\alpha S^{5/2}$ and a fit to αS^n are shown. The $S^{2.77}$ dependence found here is close to the $S^{5/2}$ dependence predicted for hk_c. The shape of the error surface in (α, n) space is broad, with only a 1 % difference in the magnitude of the r.m.s. error between the $S^{5/2}$ and S^3 fits to the data.

The local slope, hk_c, versus the input slope, S, are shown in figure 15. The dashed line has a slope of one. The dash-dot line is a fit of the data by minimizing the median square error. The slope of the fit is 1.03, consistant with an estimate of 1.1–1.2 obtained from comparison of figures 13 and 14.

While the scatter in the data in figure 14 is relatively large (a factor of 2–3), the two populations of data for spilling and plunging waves are reasonably distinct with the former occurring at lower S and showing some sign of reaching a maximum in the range $S = (0.3, 0.35)$. Comparison between the fits to the plunging data in figures 13 and 14, suggests that $hk_c \propto S^{6/5}$, which given the scatter in the data in figure 15, is not distinguishable from a linear relationship.

6. Discussion

We have proposed a simple model to scale the wave dissipation in a plunging breaking event. Within the range and scatter of the data there is good agreement between the data and the proposed scaling. The range of b encompasses all the data summarized in figure 2 except that of Phillips *et al.* (2001) which are still one to
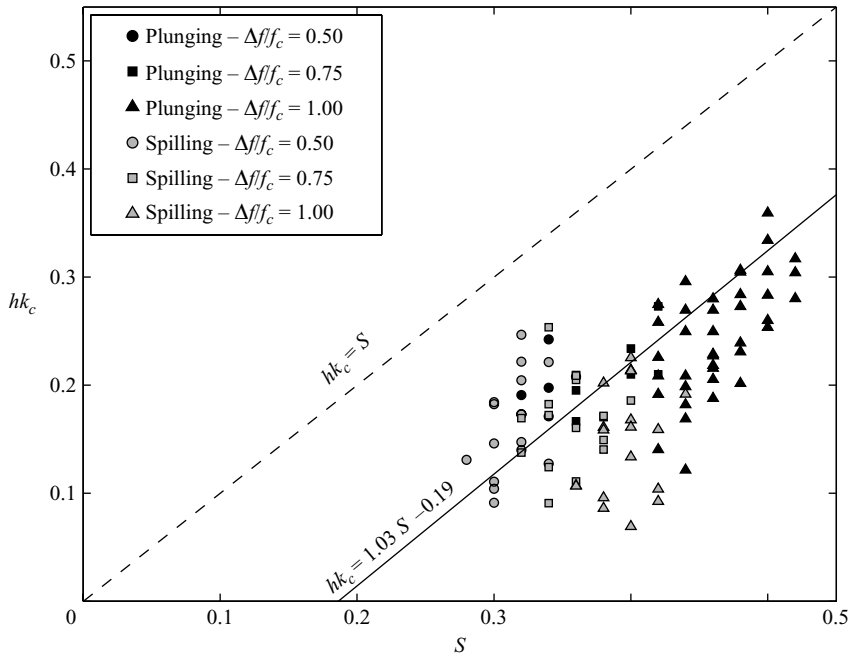
FIGURE 15. The local slope (hk_c) versus the input slope (S). The dashed line has a slope of one, while the solid line has a slope of 1.03 determined by minimizing the median square error of the data to a line. The predicted linear slope from comparison of the data shown in figures 13 and 14 is 1.11. See figures 1(*a*) and 1(*b*) for a definition of *h*.

two orders of magnitude smaller than the values of *b* found in these measurements. The reasons for this are not clear, but several factors may be involved. First the measurements of Phillips *et al.* (2001) were indirect field measurements, depending on microwave scattering to identify breaking waves. However, it is well known that shorter waves may break near the crests of longer waves and thus the speed at which the region of enhanced backscatter travels may not be a good indicator of the wavelength of the breaking waves, nor, by implication, the phase speed of the shorter breakers. Other things being equal, an overestimate of *c* in (2.8) will lead to a corresponding underestimate of *b*. However, it may also be the case that the field data correspond to smaller wave slopes than those used here, which with a 5/2 dependence would lead to correspondingly smaller *b*. For example, according to the quasi-empirical relationship $b = 0.31S^{2.77}$ from figure 14, $b = O(10^{-3})$ from Phillips *et al.* (2001) would correspond to a characteristic slope of $S = 0.13$. Similarly, field measurements by Gemmrich (2007)† with *b* estimated at $O(10^{-5})$ would correspond to $S = 0.02$, but extrapolations of our data to such low values of *b* may not be justified when taking into account the developments described immediately below. In view of the difficulties of measuring or inferring *b* from field data, laboratory measurements remain the most direct method for estimating *b* and relating the breaking kinematics to the dynamics.

In the course of final revisions of this paper for publication, two opportunities arose to broaden the scope of the material to be discussed here. First, two of us (L. L. & W. K. M.) had the opportunity to conduct focused breaking experiments

---

† We would like to thank an anonymous reviewer for bringing this article to our attention.
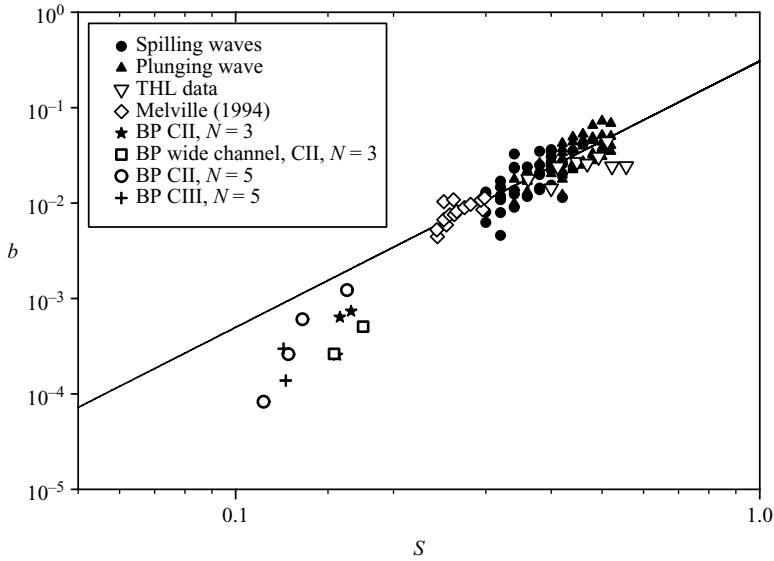
FIGURE 16. Plot of b versus S for SIO spilling and plunging waves along with the data of Melville (1994) and the THL data. Also shown are the data of Banner & Peirson (2007, BP). The solid line is a least-squares fit to the SIO data and has a slope of 2.77.

in a much larger channel at the Tainan Hydraulics Laboratory (THL), Taiwan, the details of which are described in Appendix A, with the final results included here. Secondly, Banner & Peirson (2007, hereinafter referred to as BP) published the results of laboratory experiments very similar to those described here.

The focus of BP was in measuring the evolution of wave groups to breaking to test the earlier numerical result of Song & Banner (2002) that a breaking threshold existed based on the dimensionless rate of convergence of the wave energy density in a group, δ. In doing so they found that the strength of breaking, as measured by the breaking parameter b, increased with the same slope parameter, S, as used here, and approximately linearly with the value of δ at breaking, δ_{br}. BP define

$$\delta(t) = \frac{1}{\omega_c} \frac{\mathrm{D}\langle\mu\rangle}{\mathrm{D}t}, \tag{6.1}$$

where $\mathrm{D}/\mathrm{D}t$ is the rate of change following the wave group whose mean carrier frequency is ω_c, $\mu = Ek^2$ is a non-dimensional local energy density, which is equivalent to a local slope parameter. Here, E is the wave energy density (divided by $\rho_w g$) and k is the local wavenumber. The local mean value of μ averaged over several wave periods is $\langle\mu(t)\rangle$. Since BP were interested in investigating the threshold of breaking, their values of b are expected to be small when compared with those measured here which were largely devoted to testing the inertial model for plunging breakers. However, in view of the apparent applicability of the inertial scaling of b for both spilling and plunging breakers in our experiments, it is of interest to investigate whether BP's results are consistent with this scaling. Figure 16 shows b vs. S for our SIO data, that of Melville (1994) and all of BP's data. The line, which is fitted to our data, has a slope of 2.77 and when extrapolated to the smaller slopes of BP's measurements gives values of b larger than BP's, but approximately half of their data is within the scatter of our own data relative to the extrapolated line. This is not inconsistent with

a threshold value of S for breaking, with BP's data potentially asymptoting to ours at larger values of S. While our data show that b primarily depends on S, the slope parameter, we also find a weaker dependence on the bandwidth of the wave group, consistent with our dimensional analysis going back to Melville & Rapp (1985) and RM. Also shown in figure 16 are the data from the THL experiments and data from Melville (1994) which used results from earlier experiments at MIT. Thus the THL and MIT data are consistent with the data from the SIO experiments.

The focus of BP was on the onset of breaking and testing the results of Song & Banner (2002) regarding the use of δ as a threshold for the onset of breaking and collapsing the data for b. The use of a dimensionless rate of increase of the energy density, or equivalently the rate of increase of a local slope parameter, to correlate with the strength of breaking is intuitively very appealing and offers physical insight into the evolution to breaking. However, its local definition attracts the same potential criticism as does our use of hk_c in the inertial argument: that it has no *a priori* ability to predict the onset of breaking since it requires the measurement of local variables at breaking. Furthermore, measuring derivatives of local variables is an inherently noisy process. However, the attractiveness of the basic idea prompts the question: Can we use an estimate of the rate of convergence of the energy density at breaking, based on *a priori* knowledge, to collapse the data from BP and our data?

Notwithstanding the role of nonlinearity in the breaking process, all of our experimental designs for wave breaking experiments based on dispersive focusing have used linear theory to estimate the location and time of breaking to within a wavelength and a wave period. This suggests that a linear estimator of the rate of energy convergence based on *a priori* information may prove useful in correlating the data for b. A version of δ at breaking based on linear wave dynamics,

$$\delta_{lb} = \frac{c_{gc} k_c^4 x_b E_0}{4\pi^2 \sigma_c},$$ (6.2)

is developed in Appendix B. Figure 17 shows our (SIO and THL) data along with the BP data plotted against δ_{lb}. While the data sets do not have overlapping values of δ_{lb} continuously extrapolating between the data sets appears plausible. Again it should be emphasized that whereas BP approached the problem from the onset of breaking at smaller values of δ_{lb}, we approached it with the aim of testing the inertial model of dissipation for plunging breakers. Indeed, our data, especially the THL data, show some signs of reaching saturation in the values of b for the strongest breaking waves. The dependence of b on δ_{lb} is not linear as was found for b and δ_{br} by BP, but we would not expect it to be since δ_{lb} is not linearly related to δ_{br}. Also, it must be conceded that the use of δ_{br} does a better job of collapsing the BP data than does δ_{lb}, but this still leaves the issue of predictability since δ_{br} is not known *a priori*.

As mentioned previously, the inertial estimate of the dissipation rate gives us only an order of magnitude estimate. We found that $\epsilon = \chi u^3 / l$ for plunging waves yielded $\chi = 0.32 - 0.47$, but we wish to see how this compares with measurements of χ in the literature. Sreenivasan (1984) provides measurements of χ in grid-generated turbulence and finds that χ tends to 0.43 for $R_\lambda > 50$, where R_λ is the Taylor microscale Reynolds number. The Taylor microscale Reynolds number is defined as $\langle u^2 \rangle^{1/2} \lambda / \nu$ where $\langle u^2 \rangle^{1/2}$ is an r.m.s. velocity and λ the Taylor microscale (see Drazen 2006, §IV.4). Pearson, Krogstad & van de Water (2002) extended this work to include results of typical wake flows and found that $\chi \approx 0.5$ for high R_λ. Svendsen (1987) has shown that breaking, waves in the surf zone have turbulence characteristics similar to plane wakes. As is shown in Drazen (2006), approximately
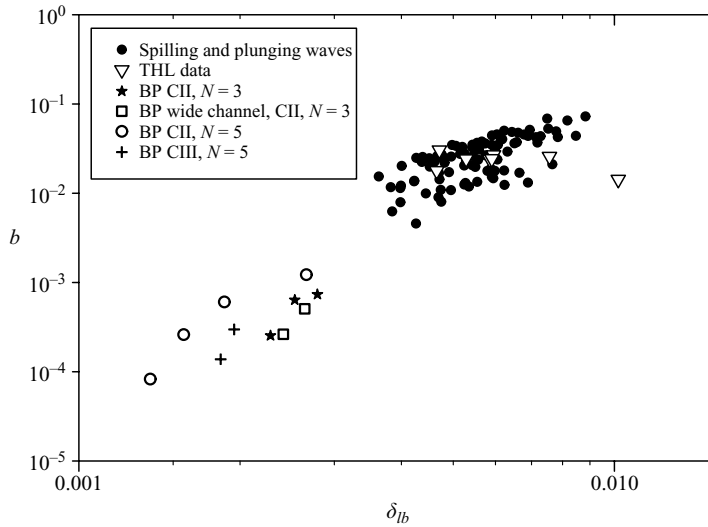
FIGURE 17. Plot of b versus δ_{lb} for SIO spilling and plunging waves, along with THL data and that of Banner & Peirson (2007).

3.5 wave periods after breaking, $R_\lambda \approx 600$ for the plunging wave considered. The fact that the values of χ implied by our data are within a factor of $0.9 - 1.6$ of other measurements in the literature, provides additional support for the use of inertial estimates of dissipation for breaking waves.

Finally, it is worth commenting on the potential application of the results of this work. As mentioned in §1, improved models of wave dissipation are required for numerical modelling of surface waves in coupled atmosphere–ocean models. DNS and LES modelling by Sullivan *et al.* (2004) and Sullivan *et al.* (2007) shows that the explicit inclusion of breaking in marine boundary-layer models may lead to qualitative differences in the kinematics and dynamics throughout the boundary layer. Breaking leads to a loss of energy from the wave field and is a source of energy for the turbulent marine boundary layer. The overall momentum and energy fluxes from waves to currents and turbulence for a region of the ocean surface depend on both the statistics of wave breaking, as formulated by Phillips (1985), and the dynamics of individual breakers as considered here. The statistics of breaking cannot be reproduced in the laboratory, except perhaps at the smallest scales, and so field measurements are necessary to both motivate and test statistical theories of breaking. Melville & Matusov (2002) and Gemmrich (2005) have used video imagery to directly measure $\Lambda(\boldsymbol{c})\,\mathrm{d}\boldsymbol{c}$. Melville, Romero & Kleiss (2005) demonstrated that concurrent airborne video imagery and surface elevation profiles using a scanning LIDAR could be used to identify breaking waves, their kinematics (through the phase velocity $\boldsymbol{c}$) and the local spatial wave profile. Thus, in principle, we can now measure breaking waves with visible (whitecap) signatures in the field, but the coupling between the kinematics and the dynamics is through the breaking parameter b, which cannot be directly measured in the field. Further work is required to relate the measurement of b in the laboratory to models and measurements of breaking in the field.

Appendix A. Tainan Hydraulics Laboratory experiments

During the course of writing this paper in April 2007, two of us (L. L. & W. K. M.) had the opportunity to conduct similar experiments to those at SIO at the Tainan Hydraulics Laboratory (THL), National Cheng-Kung University, Taiwan. The 'Supertank' is approximately 300 m long, 5 m wide, and 5.2 m deep, and for these experiments the water depth was 3 m. Waves were generated with a computer-controlled hydraulically driven piston-type wavemaker at one end of the channel and dissipated on a 1:20 slope beach at the other end, for a total constant depth section of 200 m starting from the resting position of the wave paddle.

Breaking waves were generated at a distance of 40–50 m from the wavemaker using two types of breaking-wave-generation technique. The first is the dispersive focusing method used at SIO (see § 3.3 for more details): wave packets were composed of 32 separate wave components of constant slope ak, and centre frequency $f_c = 0.6$ Hz, and a bandwidth $\Delta f = 0.6$ Hz. The second method is based on the same principle, but in the time domain. Consider the free-surface displacement at the paddle, $\eta(0, t)$, as

$$\eta(0, t) = a(t)\mathrm{e}^{\mathrm{i}\phi(t)}, \tag{A 1}$$

where $a(t)$ and $\phi(t)$ represent the instantaneous amplitude and phase, respectively. The instantaneous radial frequency $\sigma(t)$ is defined by

$$\sigma(t) = \frac{\partial \phi(t)}{\partial t}. \tag{A 2}$$

Assuming a wave packet of given centre frequency σ_c and bandwidth $\delta\sigma$, the instantaneous radial frequency σ at the paddle can be written as

$$\sigma(t) = \left(\sigma_c + \frac{\delta\sigma}{2}\right) - \delta\sigma \frac{t}{T_o}, \tag{A 3}$$

where T_o is the duration of the wave packet that determines the location and time of breaking x_b and t_b. Integrating $\sigma(t)$, we obtain

$$\phi(t) = \left(\sigma_c + \frac{\delta\sigma}{2}\right) t - \delta\sigma \frac{t^2}{2T_o} + \phi_0, \tag{A 4}$$

where ϕ_0 is an arbitrary constant. $a(t)$ is then calculated assuming the deep-water dispersion relationship and a wave packet of constant slope $a(t)k(t) = \alpha$ where $\alpha = S/N$ and N is the number of wave components.

Generated wave packets were composed of 32 wave components, centre frequency of 0.6 Hz and bandwidth of 0.4 to 0.6 Hz. The wavemaker transfer function was quantified at different locations in the tank, using wave gauges to estimate the wave amplitude and phase response to monochromatic forcing.

Surface displacement measurements were made using 31 resistance wire wave gauges, and 8 ultrasonic wave gauges (Banner QT50U) synchronously recorded at 50 Hz. Gauges were mounted approximately 30 cm from the side of the channel, approximately 4 to 5 m apart, with the first located 15 m away from the paddle, and the last 169 m away. The wire wave gauge data used here were dynamically calibrated against the ultrasonic wave gauges. The duration of breaking was measured using a hydrophone (Bruel and Kjaer, Type 2635) positioned at the breaking location, at a depth of approximately 2 m, sampled at 10 kHz and synchronized with the wave gauge measurements.

Appendix B. The rate of energy convergence based on linear dynamics

For similar wave focusing experiments to those we have described here, following Song & Banner (2002), BP suggest that the onset of breaking and the breaking parameter b can be correlated with an associated non-dimensional parametric mean growth rate $\delta(t)$, defined by (6.1). BP show that the threshold of breaking occurs for $\delta_{br} = 0.0014$, consistent with Song & Banner (2002). They also find that in the range of their experiments, the breaking parameter $b \propto \delta$ at breaking. While these results give useful insight into the processes related to breaking, like our correlation of b with hk_c, they are not predictive since they depend on parameters that are not known *a priori* but must be measured at breaking, whether it be in numerical or physical experiments. Furthermore, in the case of BP, it depends on taking gradients of the measured variables, which is inherently noisy. This raises the question of whether a different parameter that contains the essential physical content of δ, can be based on *a priori* information. From dimensional analysis of the same problem dating back to Melville & Rapp (1985) and RM we know that the evolution of the wave packet has a parametric dependence on a measure of the wave slope, the bandwidth and the distance to breaking. The question is whether we can define a parameter for the rate of energy focusing at breaking based on linear dynamics. The fact that linear dynamics gives a good approximation of the time and location of breaking, suggests that strong nonlinear effects are only significant in the immediate vicinity of breaking.

Our experiments and those of BP can be represented by a wave channel extending from $x = 0$ along the x-axis. At $x = 0$, a focusing wave packet is generated from $0 \leqslant t \leqslant T_0$ with wave components having group velocities in the range $c_{g1} \leqslant c_g \leqslant c_{g2}$. According to linear theory the wave packet will focus at (x_b, t_b), where

$$t_b = \frac{c_{g2} T_0}{c_{g2} - c_{g1}}, \tag{B 1}$$

$$x_b = c_{g1} t_b = \frac{c_{g1} c_{g2} T_0}{c_{g2} - c_{g1}}. \tag{B 2}$$

The duration of the wavepacket, the time between the two limiting rays, as a function of x, is given by

$$t_2 - t_1 = T_0 \left(1 - \frac{x}{x_b} \right). \tag{B 3}$$

To leading order for a narrow-banded wave packet, the local energy density (divided by $\rho_w g$) averaged over the duration of the wave packet, $E(x)$, is given by

$$E(x) = \frac{E_0}{1 - \frac{x}{x_b}}. \tag{B 4}$$

Following Song & Banner (2002), we define a version of their δ parameter based on linear wave dynamics,

$$\delta_l(x) = \frac{c_{gc}k_c^2}{\omega_c}\frac{\mathrm{d}E(x)}{\mathrm{d}x} = \frac{c_{gc}k_c^2}{\omega_c x_b}\frac{E_0}{\left(1 - \frac{x}{x_b}\right)^2}. \tag{B 5}$$

Consistent with linear theory, there is a singularity at $x = x_b$, but we can define a representative breaking value for δ_l at $x = x_b - \lambda_c$, where λ_c is the wavelength at the centre frequency of the wave packet. This is consistent with the constraint that the nonlinear focusing will result in at least one wave in the packet. Thus

$$\delta_{lb} = \frac{c_{gc}}{2\pi c_c}\frac{x_b E_0 k_c^2}{\lambda_c} = \frac{c_{gc} x_b k_c^4 E_0}{4\pi^2 \sigma_c}. \tag{B 6}$$

For deep-water waves, this can be written

$$\delta_{lb} = \frac{x_b E_0 k_c^2}{4\pi \lambda_c}. \tag{B 7}$$

Thus we can define a parameter *a priori* which is qualitatively consistent with the essential physical ideas of Song & Banner (2002) and BP, but does not depend on knowing various parameters at breaking. However, it does not capture the effects of the nonlinear dynamics that are expected to be significant close to breaking.

Note that $E_0 k_c^2$ is a slope parameter and x_b/λ_c is a dimensionless measure of the distance to breaking. For small bandwidth, δk, this may be approximated by

$$\frac{x_b}{\lambda_c} \approx 2\frac{k_c}{\delta k}\frac{c_{gc}T_0}{\lambda_c}, \tag{B 8}$$

which apart from the factor of two is the product of the reciprocal bandwidth and a measure of the number of waves in the packet at $x = 0$.

REFERENCES

BANNER, M. L. & PEIRSON, W. L. 2007 Wave breaking onset and strength for two-dimensional deep water waves groups. *J. Fluid Mech.* **585**, 93–115.

BANNER, M. L. & PEREGRINE, D. H. 1993 Wave breaking in deep water. *Annu. Rev. Fluid Mech.* **25**, 373–397.

DEANE, G. B. & STOKES, D. 2002 Scale dependence of bubble creation mechanisms in breaking waves. *Nature* **418**, 839–844.

DRAZEN, D. A. 2006 Laboratory studies of nonlinear and breaking surface waves. PhD thesis, University of California, San Diego.

DRAZEN, D. A. & MELVILLE, W. K. 2008 Inertial estimates of dissipation in unsteady breaking waves. *J. Fluid Mech.* (Submitted).

DUNCAN, J. H. 1981 An experimental investigation of breaking waves produced by a towed hydrofoil. *Proc. R. Soc. Lond.* A **377**, 331–348.

DUNCAN, J. H. 1983 The breaking and non-breaking wave resistance of a two-dimensional hydrofoil. *J. Fluid Mech.* **126**, 507–520.

DUNCAN, J. H. 2001 Spilling breakers. *Annu. Rev. Fluid Mech.* **33**, 519–547.

FEDOROV, A. & MELVILLE, W. K. 1998 Nonlinear gravity–capillary waves with forcing and dissipation. *J. Fluid Mech.* **354**, 1–42.

GEMMRICH, J. 2005 On the occurrence of wave breaking. In *Rogue Waves, Proc. Aha Hulikoa Hawaiian Winter Workshop* (ed. P. Müller & D. Henderson), pp. 123–130.

GEMMRICH, J. 2007 Momentum flux and energy dissipation associated with breaking waves. In *Transport at the Air–Sea Interface – Measurements, Models and Parameterizations* (ed. C. S. Garbe, R. A. Handler & B. Jähne), pp. 133–144. Springer.

KOMEN, G. J., HASSELMANN, S. & HASSELMANN, K. 1984 On the existence of a fully developed wind–sea spectrum. *J. Phys. Oceanogr.* **14**, 1271–1285.

LAMARRE, E. & MELVILLE, W. K. 1991 Air entrainment and dissipation in breaking waves. *Nature* **351**, 469–472.

LIGHTHILL, J. 1978 *Waves in Fluids*. Cambridge University Press.

LOEWEN, M. R. 1991 Laboratory measurements of the sound generated by breaking waves. PhD thesis, MIT/WHOI Joint Program.

LOEWEN, M. R. & MELVILLE, W. K. 1991 Microwave backscatter and acoustic radiation from breaking waves. *J. Fluid Mech.* **224**, 601–623.

LONGUET-HIGGINS, M. S. 1974 Breaking waves in deep or shallow water. In *Proc. 10th Symp. on Naval Hydrodynamics* (ed. R. D. Cooper & S. D. Doroff), pp. 597–605. Office of Naval Research, Arlington, Virginia.

MELVILLE, W. K. 1994 Energy dissipation by breaking waves. *J. Phys. Oceanogr.* **24**, 2041–2049.

MELVILLE, W. K. 1996 The role of surface-wave breaking in air–sea interaction. *Annu. Rev. Fluid Mech.* **28**, 279–321.

MELVILLE, W. K. & MATUSOV, P. 2002 Distribution of breaking waves at the ocean surface. *Nature* **417**, 58–63.

MELVILLE, W. K. & RAPP, R. J. 1985 Momentum flux in breaking waves. *Nature* **317**, 514–516.

MELVILLE, W. K., VERON, F. & WHITE, C. 2002 The velocity field under breaking waves: coherent structures and turbulence. *J. Fluid Mech.* **454**, 203–233.

MELVILLE, W. K., ROMERO, L. & KLEISS, J. M. 2005 Extreme wave events in the Gulf of Tehuantepec. In *Rogue Waves, Proc. Aha Hulikoa Hawaiian Winter Workshop* (ed. P. Müller & D. Henderson), pp. 23–28.

PEARSON, B. R., KROGSTAD, P.-Å & VAN DE WATER, W. 2002 Measurements of the turbulent energy dissipation rate. *Phys. Fluids* **14** (3), 1288–1290.

PERLIN, M., HE, J. & BERNAL, L. P. 1996 An experimental study of deep water plunging breakers. *Phys. Fluids* **8** (9), 2365–2374.

PHILLIPS, O. M. 1985 Spectral and statistical properties of the equilibrium range in wind-generated gravity waves. *J. Fluid Mech.* **156**, 505–531.

PHILLIPS, O. M., POSNER, F. L. & HANSEN, J. P. 2001 High range resolution radar measurements of the speed distribution of breaking events in wind-generated ocean waves: surface impulse and wave energy dissipation rates. *J. Phys. Oceanogr.* **31**, 450–460.

RAPP, R. J. & MELVILLE, W. K. 1990 Laboratory measurements of deep-water breaking waves. *Phil. Trans. R. Soc. Lond.* A **331**, 735–800.

SONG, J. B. & BANNER, M. L. 2002 On determining the onset and strength of breaking for deep water waves. Part 1: Unforced irrotational wave groups. *J. Phys. Oceanogr.* **32**, 2541–2558.

SREENIVASAN, K. R. 1984 On the scaling of the turbulence energy dissipation rate. *Phys. Fluids* **27** (5), 1048–1051.

SULLIVAN, P. P., MCWILLIAMS, J. C. & MELVILLE, W. K. 2004 The oceanic boundary layer driven by wave breaking with stochastic variability. Part 1. Direct numerical simulations. *J. Fluid Mech.* **507**, 143–174.

SULLIVAN, P. P., MCWILLIAMS, J. C. & MELVILLE, W. K. 2007 Surface gravity wave effects in the oceanic boundary layer: large-eddy simulation with vortex force and stochastic breakers. *J. Fluid Mech.* **593**, 405–452.

SVENDSEN, I. A. 1987 Analysis of surf zone turbulence. *J. Geophys. Res.* **92** (C5), 5115–5130.

VAN DORN, W. G. & PAZAN, S. E. 1975 Laboratory investigation of wave breaking. Part ii: Deep water waves. *Advanced Ocean Engng Lab. Rep.* 71 75–21. Scripps Institution of Oceanography.